Available online at www.sciencedirect.com
ScienceDirect
ELSEVIER
Progress in Natural Science: Materials International 21(2011) 277−285
Progress in Natural Science: Materials International
www.elsevier.com/locate/pnsc

Deformation heterogeneity of Ti under cryogenic channel-die compression

K. H. KIM[1], Y. B. CHUN[2], S. K. HWANG[1]

1. Division of Materials Science and Engineering, Inha University, Incheon 402-751, South Korea;
2. ARC Centre of Excellence for Design in Light Metals, Department of Materials Engineering, Monash University, VIC 3800, Australia

Received 15 June 2011; accepted 22 July 2011

Abstract: Commercial purity Ti was subjected to channel die compression in liquid nitrogen for the purpose of studying its deformation characteristics from the viewpoint of the grain refinement induced by severe plastic deformation. Deformed specimens showed microstructural heterogeneity in that the initial blocky grains of about 50 μm in size turned into a mixture of the easily deforming soft grains and the hard grains revealing local concentration of dislocations and deformation twins. Using electron back scattered diffraction analysis the in-grain misorientation-axis distribution was studied, from which it was found that the deformation heterogeneity resulted from the anisotropy of individual grains with respect to the compression die: while the soft grains were those oriented favorably for the prism <*a*> slip, the hard ones were oriented for non-prism slips and deformation twinning. The difference in the response of individual grains, therefore, led to a remarkable effect of the crystal texture of specimens on the maximum strain that can be imposed on specimens without cracking. Based on the present results, a way to achieve expedient grain refinement through the cryogenic plane-strain compression was suggested.
Key words: titanium; cryogenic; deformation; texture; microstructure

1 Introduction

As a means to refine the microstructure of metallic materials, many researchers investigated the severe plastic deformation (SPD) in the past few decades. In his pioneering work on the equal channel angular pressing (ECAP) of pure Ni, SEGAL [1] reported that the microstructural refining occurred during ECAP in the ways characteristic to the strain path, the principles of which were delineated comprehensively in the review made by VALIEV and LANGDON [2]. HUMPHREYS et al [3] documented the criteria concerning the grain boundary properties for developing a stable fine-grain microstructure by the large strain deformation. Successful attempts abound in the methods of deformation as well as the variety of the target metals. For Ti, ECAP was studied by ALEXANDROV et al [4], STOLYAROV et al [5] and SHIN et al [6], with significant microstructural refinement. Most of these works, however, involved working at an elevated temperature, around 350 ^{o}C, to accumulate sufficient strain, about 4, for the grain refinement. In this context, the success of the room temperature equal-channel angular pressing of Ti by ZHAO et al [7] is notable. The elevated temperature operation of ECAP involves cumbersome and costly processing such as heating the processing apparatus. An alternative approach to introduce a nano-scale bimodal microstructure was suggested by WANG et al [8] for Cu. In this route, specimens were rolled at a cryogenic temperature, up to a thickness reduction of about 95% and then partially recrystallized at a low temperature. The cryogenic deformation, at a relatively low strain level, suppresses dynamic recovery to allow a high level of deformation-induced defects needed for grain refinement. The bimodal microstructure consisting of a minor volume of coarse grains within the matrix of fine grains enhanced the work-hardening capacity of the material so that the tensile elongation increased significantly. LEE et al [9] and VENKATESAN et al [10] also found that the tensile strengths of pure Al as well as Al-alloys were enhanced efficiently by the cryo-rolling. HUANG and PRANGNELL [11] also reported a grain size as small as 150 nm in an Al-Mg alloy by heavy cryogenic deformation. For hcp metals such as Mg and Ti, the SPD

Corresponding author: S. K. HWANG; Tel: 82-10-7119-7537; E-mail: skhwang2@inha.ac.kr

involves sensitive variation of the crystallographic texture. AGNEW et al [12−13] documented in detail the texture development in Mg-alloys while ZENG et al [14] and NEMAT-NASSER et al [15] presented the materials and deformation conditions leading to activation of the particular slip or twinning systems. Despite these works and other valuable works on the texture of hcp metals [16−20] it has not been disseminated so far how the materials anisotropy may be incorporated into the deformation condition in exploring the possibility of the cryogenic SPD of Ti.

We have reported earlier that the severe cryogenic deformation of V and Ti could significantly reduce the grain size and subsequently enhance the tensile properties [19]. In the present work, we studied the mechanism of the cryogenic deformation of Ti in more details to propose a way for the efficient grain refinement. Specifically, we examined the behaviors of individual grains in the context of their crystal anisotropy with respect to the mode of the cryogenic deformation. Most of all, we hoped to answer the question on the cause of the microstructural heterogeneity in deformed specimens and its implication on the cryogenic SPD approach targeted for Ti.

2 Experimental

The material used in the present study was polycrystalline Ti of Grade 2 with a nominal purity of 99.7% and the residual impurities of 0.148% (mass fraction) O, 0.094% Fe, 0.02% C and 0.001% N. Hot rolled and annealed (880 °C) Ti plates of 350 mm×350 mm×26 mm in dimension were procured from the ATI Allegheny Lundlum and cut into specimens of a rectangular shape of 12 mm×6 mm×12 mm. The specimen dimensions were designed such that their crystal textures were related to the reference directions of the channel die, the loading direction (LD), the constrained direction (CD) and the free direction (FD). A schematic view of the plane-strain loading of a specimen block inside the die is shown in Fig. 1. For the detailed shape of the die having a channel of 12 mm in width and 40 mm height, see Ref. [21]. The CrCDC was conducted with the die and specimen immersed in liquid nitrogen without lubricant at the compression rate of 0.86 mm/s. Due to the constraining action of the channel walls, the plane-strain compression was confined to only LD and FD. During the deformation the temperature of the liquid nitrogen bath was maintained below −190 °C. XRD (X-ray Diffraction) analysis of the texture was conducted in a Rigaku-RINT2500 machine with a multipurpose attachment while EBSD (Electron back scattered diffraction) data were obtained by a Hitachi 4300 SEM-FEG and analyzed with a TSL-OIM software program. Using the EBSD, the standard IPF (Inverse pole figure) map and the orientations of individual grains with respect to the reference directions of the CrCDC die were obtained. Also, from the EBSD analysis, the data on the IGMA (In-Grain Misorientation Axes) distributions due to the deformation-induced crystal misorientation in individual grains were extracted and were presented by stereographic projections with the three-pivot orientations, [0001], $[10\bar{1}0]$ and $[2\bar{1}\bar{1}0]$.

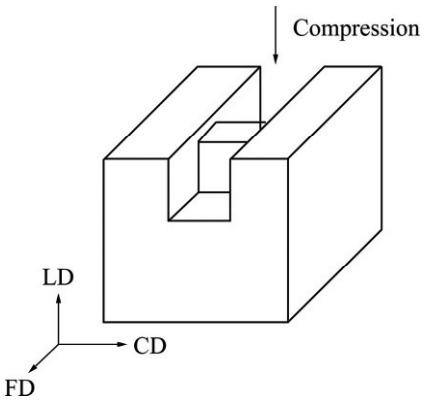

Fig. 1 Schematic view of plane-strain compression of a specimen block placed inside die (LD: Loading direction; FD: Free direction; CD: Constrained direction)

3 Results

The initial microstructure of specimens prior to the cryogenic compression consisted of blocky grains of approximately 50 μm in the average size. These grains appeared as equiaxed ones in the normal cross section of the original plate but as flattened lamellae in the transverse section, as shown in Fig. 2. The orientations

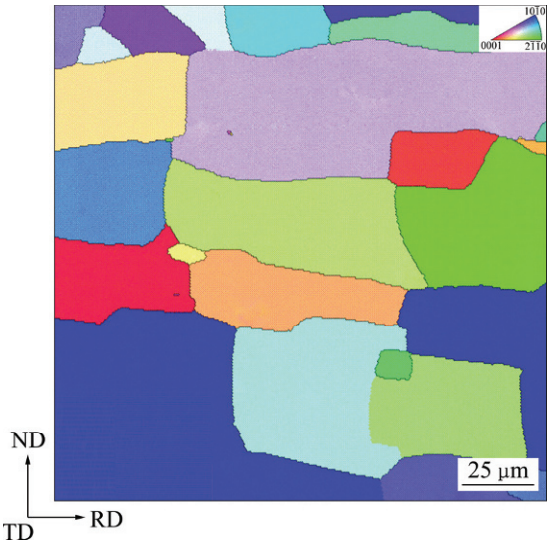

Fig. 2 EBSD-IPF map of transverse section of original Ti plate, alpha-annealed (Refer to the color code of the inset stereographic projection for orientations of individual grains)

of individual grains are color-coded such that the red, blue and green grains have their [0001], $[10\bar{1}0]$ and $[2\bar{1}\bar{1}0]$ orientations, respectively, to the transverse direction (TD) of the original plate.

The texture of the initial microstructure may be termed as a 'bimodal basal texture', in which (0002) poles pointed toward the directions tilted symmetrically by about 30° from the plate normal direction toward the transverse direction. Also, there was a preferred intensity of the $(10\bar{1}0)$ poles toward the rolling direction. The details of the texture, as analyzed by XRD, are presented in Fig. 3. This type of texture has been well known in the literature (e.g. see Ref. [22]) and it represents the alpha-annealed state of Ti as well as Zr.

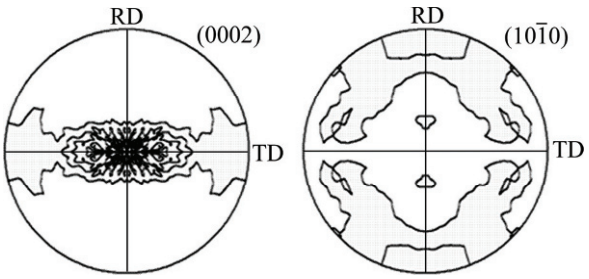

Fig. 3 Pole figures of starting material, CP-Ti plate in a hot rolled and annealed condition (Left: (0002); Right: $(10\bar{1}0)$; RD: Rolling direction; TD: Transverse direction; Max. intensity: 4.5 for (0002), 2.5 for $(10\bar{1}0)$)

Since the specimens for the cryogenic deformation were machined out of the textured annealed plates they exhibited different textures depending on the specimen geometry with respect to the reference directions of the CrCDC die. Hence it was necessary to designate the specimen anisotropy: for simplicity, the orientation of the majority of the (0002) poles in the specimen was aligned with one of the reference directions of the die. A schematic illustration of the three different specimen types is shown in Fig. 4 using a direct pole figure. Thus each specimen was characterized by the orientation of the basal planes and the easiness of the prismatic slip in each case, as described in Fig. 5. For the grains of C-type, Fig. 5(a), with their *c* axes parallel to the constrained direction, prismatic slips occur easily on the grains with their $(10\bar{1}0)$ planes inclined toward the loading (L) direction by 60°. In this case, the Schmid factor for the prismatic slip is about 0.43. For the F-type grains, Fig. 5(b), the Schmid factor is the same as the C-type grains; however, the slip is constrained by the die wall. For the L-type grains, Fig. 5(c), the Schmid factor is zero for the prismatic slip, thus it is likely that other mode of deformation will be activated. In this respect, the F-type specimen and the L-type specimen configurations may be called as the '*c*-axis extension' specimen and '*c*-axis compression' specimen, respectively.

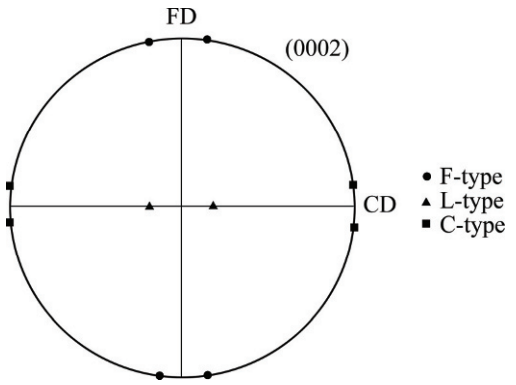

Fig. 4 Designation of CrCDC specimen orientations based on alignment of (0002) poles with respect to reference directions of channel die (FD: Free (extension) direction; CD: Constrained direction)

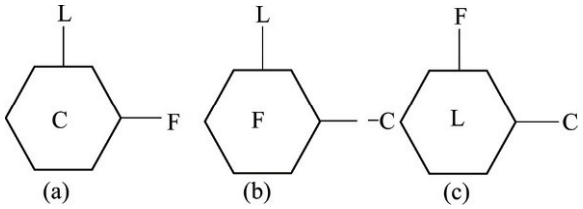

Fig. 5 Schematic configuration of orientation of basal plane in the three different types of CrCDC specimens

During CrCDC, the maximum strain deliverable to specimens without cracking and the mode of deformation are the important factors for the effective grain refinement through SPD. Due to the texture inherent in the original α-annealed Ti plates, specimens cut out from these plates inherited the anisotropy, thus the specimens subject to CrCDC exhibited varying degrees of the maximum fracture strain. We attempted to correlate the maximum fracture strain with the specimen anisotropy as represented by the alignment of the (0002) poles.

In Fig. 6, the maximum strain attainable during CrCDC is shown as a function of the specimen anisotropy. The L-type specimens as well as F-type specimens could absorb up to about 0.5 in the equivalent strain, beyond which specimens cracked. In contrast, the C-type specimens could endure a strain of up to 1.3 without cracking. This result clearly demonstrates that the deformability of specimens was sensitively affected by the orientation of the basal poles. PAUL et al [23] found that the grain orientations of a bi-crystal Al affected the mode of deformation significantly during CrCDC. NAVE and BARNETT [24] also reported a significant texture dependence of the fracture strain in Mg plane-strain compressed at room temperature.

The rationale for the correlation between the

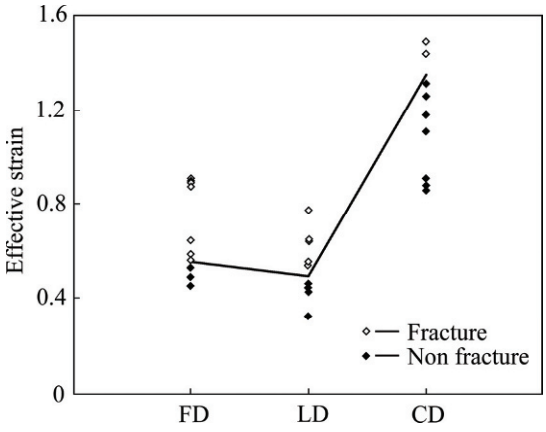

Fig. 6 Effect of specimen texture on fracture strain of specimens during cryogenic plane-strain compression (FD, LD and CD refer to the specimens defined as F-type, L-type and C-type, respectively in the text)

maximum fracture strain and the specimen anisotropy was sought in terms of the deformation mechanism. To study the deformation mechanisms, we employed an experimental approach based on the analysis of the slip-induced lattice rotation. The theory of this approach was first introduced in the 1960s by RAPPERPORT and HARTLEY [25] to determine the slip systems of Zr single crystals. In their work, the authors analyzed the asterism at the Laue spots for the deformed specimens and deduced the slip systems under the assumption that the asterism arose from bending of the crystal lattice planes under the action of slip. The bending was assumed to take place about an axis termed as the Taylor axis. In an earlier work [24] we reported that the analysis of the IGMA distributions could be used to determine the slip systems in CP-Ti. The technique, which essentially determines the rotation axes of the lattices using the EBSD, was also used in the present work.

The Taylor axis, $\boldsymbol{T}$, is a vector cross product of the slip plane normal, $\boldsymbol{n}$, and the slip direction, $\boldsymbol{a}$, thus

$$\boldsymbol{T}=\boldsymbol{n}\times\boldsymbol{a} \quad (1)$$

In Ti, the most active slip system is the prism <*a*> slip, i.e., $\{10\bar{1}0\}\langle 11\bar{2}0\rangle$, in which case $\boldsymbol{T}$ is $\langle 0001\rangle$. Therefore, if the IGMA distribution is preferentially focused around $\langle 0001\rangle$ then it may be deduced that the prism slip was activated.

Using the EBSD method, we examined the IGMA distribution characteristics of all the specimens deformed under the CrCDC. In this analysis, specimens were deformed up to a strain of only 0.33 because the OIM (Orientation image mapping) quality of EBSD pattern diminished with severer deformation. The IGMA analysis was conducted on many individual grains for the three different types of specimens, and a typical result is shown as the stereographic projections in Figs. 7, 8 and 9.

Fig. 7 shows the image and the orientations of individual grains and their IGMA distributions of an L-type specimen. Due to the specimen anisotropy shown in Fig. 4, the specimen type such as C, L and F have greater portions of grains with their (0002) poles oriented toward the CD, LD and FD of the die, respectively. However, there were more grains oriented otherwise. Therefore the IGMA distributions in Fig. 7 are specific to the individual grain orientations. For example, grain A was of a C-type and the spot images of the poles showed

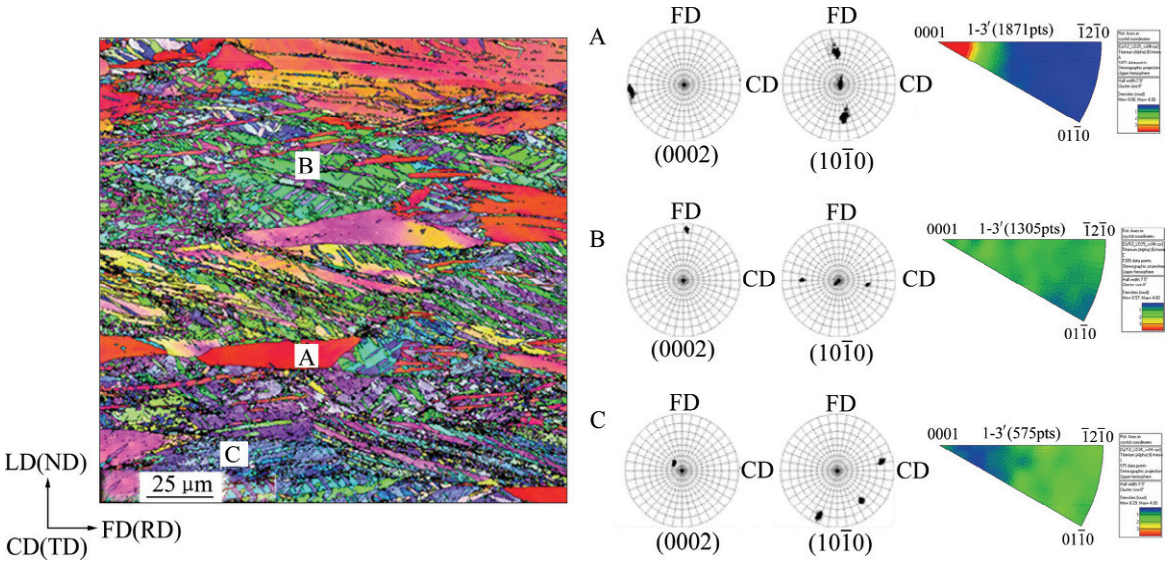

Fig. 7 EBSD-IPF map of an L-type specimen cryogenic plane-strain compressed by an effective strain of 0.33 (left), pole figures of selected grains (middle) and stereographic projections of IGMA (right) (Deformation twins exist in grains, e.g., B, that have (0002) poles non-parallel to CD. Step size 0.2 μm, ND, RD and TD are the reference directions of original plate)

an asterism. Moreover, the stereographic projection of IGMA showed a strong concentration around the (0002) poles. On the other hand, for grains B and C, whose (0002) poles were oriented toward the FD and LD, respectively, the IGMA distributions were random. This result indicates that the prism <*a*> slip was activated dominantly in grain A while other modes of deformation, deformation twinning being one of them, were actively involved in the other two grains. The features appearing in Fig. 7 could also be confirmed in the other specimen types, F-type (Fig. 8) and C-type (Fig. 9).

In summary, the results presented in Figs. 7, 8 and 9 could be utilized to deduce the deformation mechanism of individual grains. The distinctive features for the prism slip are the asterism in the poles and the concentration of the IGMA around the [0001] direction. For the non-prism slips such as deformation twins, the image of the poles is discrete without asterism and the preferential concentration of the IGMA does not exist. Fig. 10 illustrates this point schematically.

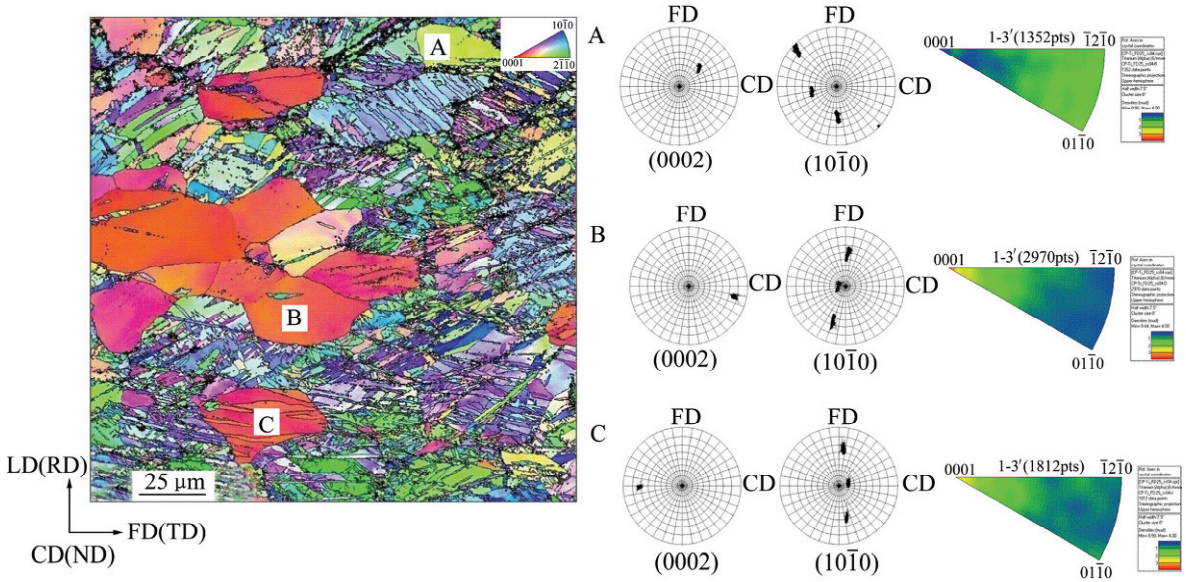

Fig. 8 EBSD-IPF map of an F-type specimen cryogenic plane-strain compressed by an effective strain of 0.25 (left), pole figures of selected grains (middle) and stereographic projections of IGMA (right) (Like in Fig. 6 and Fig. 7, the grains (D and J) with their basal normal vectors oriented toward the CD showed strong indication of prism slip. Step size 0.2 μm, ND, RD and TD are the reference directions of original plate)

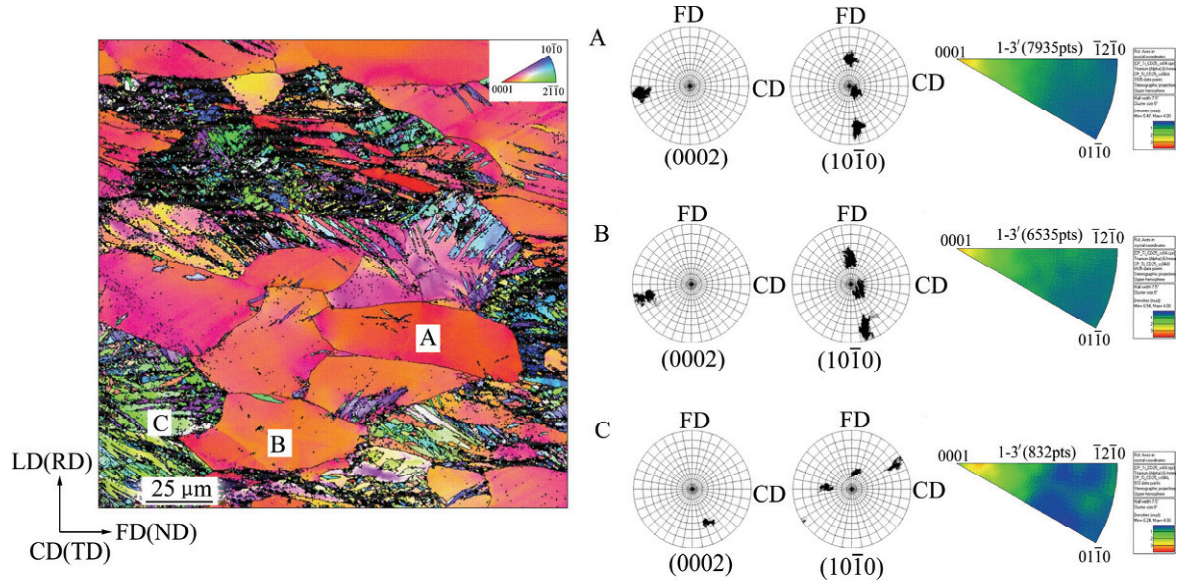

Fig. 9 EBSD-IPF map of an C-type specimen cryogenic plane-strain compressed by an effective strain of 0.25 (left), pole figures of selected grains (middle) and stereographic projections of IGMA (right) (While the grains (A, D) with the (0002) poles oriented toward the CD appear clean and high concentration of the IGMA around (0001) that (L) with the (2110) poles toward the CD show deformation twins. Step size 0.2 μm, ND, RD and TD are the reference directions of original plate)

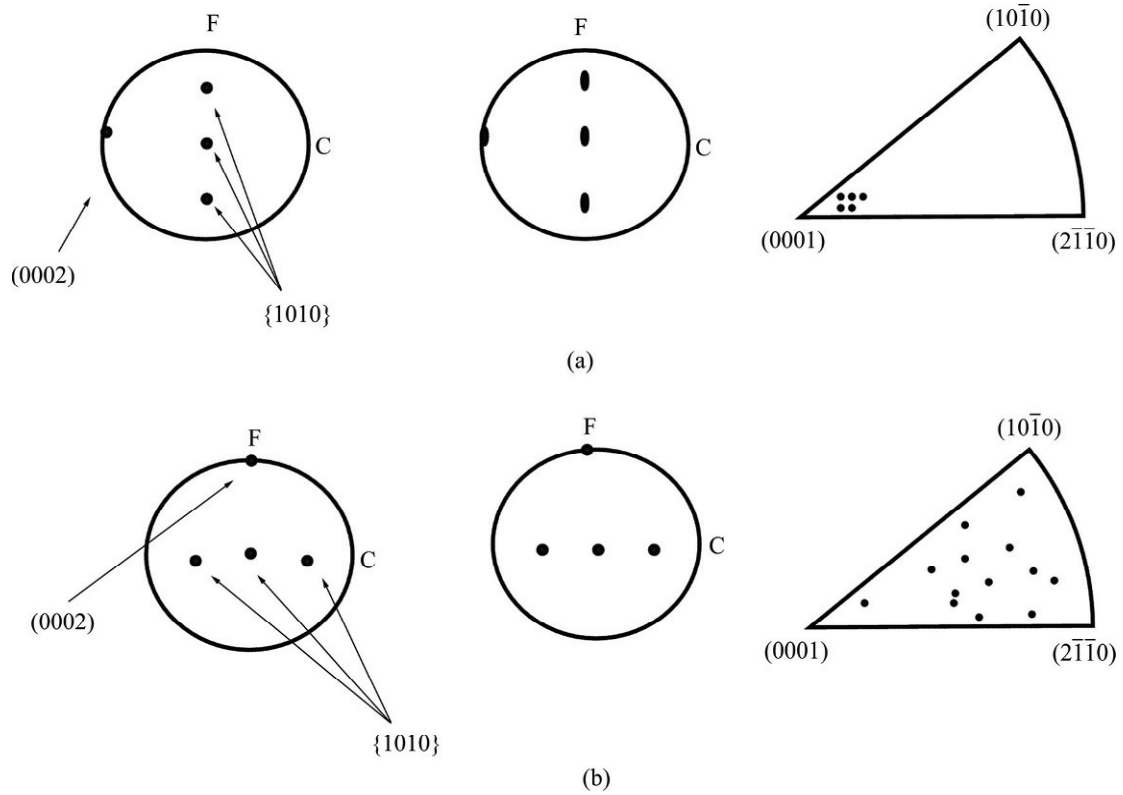

Fig. 10 Schematic illustration of the images of (0002) and $(10\bar{1}0)$ poles of Ti prior to deformation (left) and after deformation (center), and the stereographic projection (right) of the plane cross-sectional to the CD showing the distributions of IGMA: (a) C-type specimen, exhibiting the evidence of prismatic slip causing streaking of the poles due to lattice misorientation and the preferential alignment of the basal poles toward the C direction; (b) F-type specimen, showing no pole-streaking and the absence of the preferred orientation due to the difficulty of the prism slip. The loading direction is perpendicular to the plane of the paper.

Besides the maximum fracture strain, the texture of CrCDC deformed CP-Ti varied greatly with the specimen types. In the L-type specimen, the bimodal basal texture of the initial plate was essentially maintained although the maximum intensity of the texture decreased slightly, from 4.5 to 3.6, as shown in Fig. 11(a). This is because the L-type plane-strain deformation is close to the plate rolling with the LD and FD of the CrCDC die corresponding to the ND and RD of the rolling machine, respectively, as shown in Fig. 3. There was, however, a significant change in the $(10\bar{1}0)$ poles in that CrCDC rotated them toward the FD, with a reduced maximum intensity. This is due to the difference between the rolling texture, $((0001)\langle 10\bar{1}0\rangle)$, and the annealing texture, $((0001\langle 2\bar{1}\bar{1}0\rangle)$, of Ti. In the case of the F-type specimen, the texture was notably affected by the CrCDC, as shown in Fig. 11 (b). The basal poles were rotated from the FD toward the LD, resulting in a bimodal texture symmetric along the CD as well as the FD. This was accompanied by a reduction in the maximum pole intensity from 4.5 to 3.0. The $(10\bar{1}0)$ prism poles were also rotated toward the CD at a considerably weakened intensity of 1.7. Establishment of the quadruple symmetric band texture was a consequence of the rotation of the two basal pole maxima from the FD (see Fig. 3) toward the LD. Hence the plane-strain compression in this case re-orientated the basal poles into the bimodal configuration from their starting orientation. This re-orientation, however, did not occur in the case of the C-type loading in which the basal poles had been aligned toward the CD in the starting condition. As shown in Fig. 11(c), this case led to a uniquely symmetric texture with their (0002) and $(10\bar{1}0)$ poles aligning with the CD and FD, respectively. This phenomenon is consistent with the rather clean appearance of the C-type grains in the EBSD-IPF map shown in Fig. 8. Furthermore, this supports the result of the IGMA analysis that implied dominant prism slip and consequent lattice misorientation within each of C-type grains. Therefore, the overall texture will be largely unaffected if CrCDC is conducted on a specimen in which majority of grains has its [0001] directions aligned toward the CD. For the specimens situated otherwise, the CrCDC activated non-prism slips and deformation twinning that resulted in the notable rotations of individual grains.

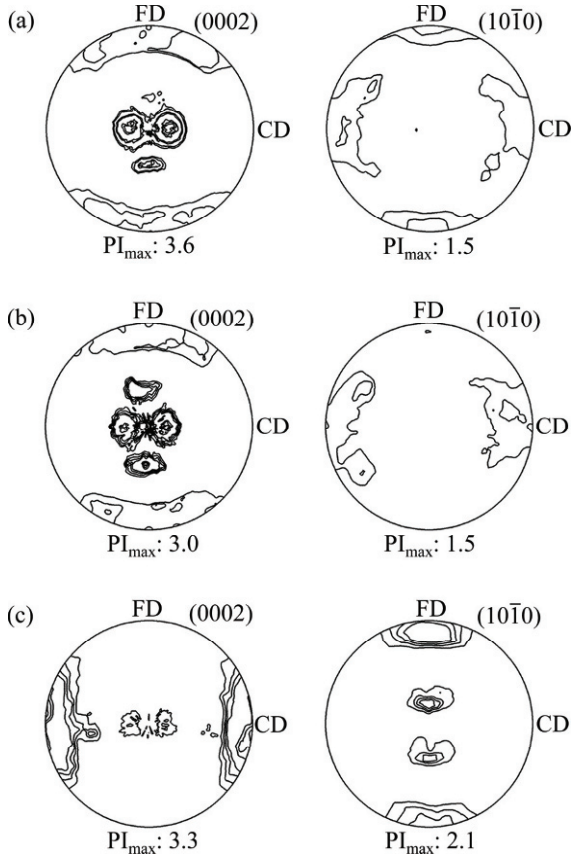

Fig. 11 Pole figures of CP-Ti CrCDC deformed: (a) L-type specimen, ε=25%; (b) F-type specimen, ε=25%; (c) C-type specimen, ε=67%, PI_{max}: maximum pole intensity

Based on the IGMA analysis of individual grains and the texture characteristics of deformed specimens, therefore, the result of the maximum fracture strain shown in Fig. 6 can be interpreted. A plane-strain compression of C-type grains activated the prism slip, which is accomplished presumably through easy glide of dislocations contained in the specimen. In this mode of deformation the grain rotation is minimal and a large plastic strain may be accommodated. Non-prism slips such as deformation twinning in the grains oriented otherwise resulted in defects such as dislocations and intersecting twin boundaries in addition to the large lattice rotation. The local accumulation of defects and twin boundary intersections provoked cracking and thus limited the fracture strain. The largest fracture strain in C-type specimens, therefore, was realized since these specimens comprised mainly of the C-type grains.

4 Discussion

In the previous work [26], we have already reported the effectiveness of the cryogenic SPD for Ti as compared to that at ambient temperature. The efficient accumulation of deformation-induced lattice defects and minimal dynamic recovery led to the ultra fine grain structure at relatively low total strain. In the present work, the main objective was to identify the deformation characteristics of individual grains under the cryogenic plane-strain compression, the information of which can be used in the future work of optimizing the strain routes for efficient grain refinement.

The texture of materials is important in the initial state as well as its evolution during SPD. As ALEXANDROV [27] and SUWAS et al [18] pointed out, it plays a crucial role in the grain refinement process. Due to the inherent texture in the starting state, Ti exhibits anisotropic behavior under any type of deformation. Furthermore, the constrained die compression studied in the present work adds to the diversity of the anisotropic behavior of specimens due to the presence of the constraining wall as well as the free deformation channel in the die. Whichever direction we cut specimens with starting texture and load them in the CrCDC die, individual grains will be activated for the slip or twinning systems chosen for the anisotropic loading condition.

Overall, the present work shows the heterogeneous nature of the deformation characteristics of individual grains. In Ti, the slip systems responsible for the plastic deformation are prism <*a*> ($\{10\bar{1}0\}\langle 11\bar{2}0\rangle$), pyramidal <*a*> ($\{1\bar{1}01\}\langle 11\bar{2}0\rangle$), pyramidal <*c*+*a*>, basal <*a*> and deformation twinning, as summarized by ZENG et al [14]. Combination of any five of these slip systems must be activated to generate a plastic strain in a specimen [28]. Among these, the most active ones at the ambient temperature and below are the prism <*a*> slip and the deformation twinning like the case reported by AKHTAR [29] in Zr, which is the main subject of discussion. When a grain receives stresses exerting a high Schmid factor for the prism <*a*> slip it will deform most smoothly and this type grain may be named as 'soft' grain. This is readily borne out from the flattened but relatively clean inner microstructure of those grains, as shown in Figs. 7, 8 and 9. These grains are of the C-type grains with their *c*-axes pointing toward the constraining wall of the die, see Fig. 5 (a), for which we confirmed the prism <*a*> slip through the IGMA analysis. For the grains oriented otherwise, i.e., the 'hard' grains, the difficulty of the prism <*a*> slip was pronounced, as revealed by the intersecting twins or dislocations of high local density, appearing as the dark contrast in the EBSD-IPF maps. It is a matter of course then to expect the easy plastic deformation in the C-type specimen because the fraction of the C-type grains in this specimen was the highest among the three different types of specimens. This explains, therefore, the variation in the maximum fracture strain of different types of specimens in Fig. 6.

As stated by HUMPHREYS et al [3], the criterion

for developing a stable microstructure in the ultra-fine grained materials during SPD is the generation of high angle grain boundaries. Although the C-type specimens showed the largest fracture strain during CrCDC, this fact does not lead to a direct conclusion that it is the best route for grain refining. The grain refinement during SPD requires a high local concentration of defects. Dislocations alone may be responsible for grain refinement: high angle boundaries can be produced by accumulation of dislocations at cell boundaries. In their equal-channel angular extrusion work of Be, FIELD et al [30] reported that successful grain refinement was achieved through dislocation activities without involving deformation twinning due to the elevated temperature of the deformation. This route of grain refinement is expected to operate in the C-type specimens. In this case, however, the total amount of deformation imposed upon specimens must be large.

For the small range of applied strain, non-C-type grains may acquire the necessary grain refining conditions earlier than the C-type ones. The dislocation structure varies with the amount of strain imposed. For example, LIU et al [31] reported that a large strain (greater than 2) in pure Al produced lamellar boundaries and incidental dislocation boundaries whereas a small strain (e.g., 0.5) dense dislocation walls and microbands. The microstructural evolution in pure Al is homogeneous, whereas, that in Ti during the CrCDC is heterogeneous. This is because the cryogenic deformation of non-C-type grains inevitably involves deformation twinning and preferential accumulation of dislocations with only a small amount of strain imposed. In their study of the low temperature (~ −100 ^{o}C) dynamic plastic deformation of Cu, LI et al [32] reported that the lamellar shape grain refinement was remarkably more efficient with deformation twinning than with the dislocation cell formation. This approach of utilizing deformation twins, however, does not preclude the adverse result of cracking at the intersections of twins or slip bands. What the preset results lead to is that a judicious combination of the strain route can be an efficient way to grain-refine the microstructure during cryogenic SPD: rotation of specimens is necessary to achieve this purpose. By way of diversifying the strain paths, one may also overcome the heterogeneity of the cryogenic deformation and thus achieve the grain refinement with the amount of strain considerably smaller than those employed in conventional SPD processes.

5 Conclusions

1) Deformation proceeded heterogeneously in that individual grains responded to the external stress differently, according to the materials texture with respect to the reference direction of press die. As a consequence, defects accumulation appeared non-uniformly throughout the specimen cross sections.

2) Two types of grain structure were identified, soft and hard. The grains situated well for the prism <*a*> slip belong to the former and the others to the latter. Compared to the soft grains, the hard ones revealed heavier accumulation of dislocations and twins, which resulted in the microstructural heterogeneity.

3) The present result suggests a way to grain-refine Ti through CrCDC efficiently: rotate specimens properly in between the multiple compressions to diversify the strain paths so that overall deformation becomes more uniform with adequate inducement of non prism slips. This will also reduce the amount of strain required for the grain refinement.

Acknowledgment

The authors wish to thank the financial support of the Korea science and engineering foundation (Basic Research Promotion Fund, KOSEF 2008-0058854) and also thank Mr. D. H. Hong for the helpful assistance in the experiment and manuscript preparation.

References

[1] SEGAL V M. Materials processing by simple shear [J]. Materials Science Engineering A, 1995, 197(2): 157−164.

[2] VALIEV R Z, LANGDON T G. Principles of equal-channel angular pressing as a processing tool for grain refinement [J]. Progress in Materials Science, 2006, 51(7): 881−981.

[3] HUMPHREYS F J, PRANGNELL P B, BOWEN J R, et al. Developing stable fine-grain microstructures by large strain deformation [J]. Philosophical Transactions of the Royal Society of London, Series A, 1999, 357(1756): 1663−1681.

[4] ALEXANDROV I V, DUBRAVINA A A, KILMAMETOV A R, et al. Texture in nanostructured metals processed by severe plastic deformation [J]. Metals and Materials International, 2003, 9(2): 151−156.

[5] STOLYAROV V V, ZHU Y T, AEXANDROV I V, et al. Grain refinement and properties of pure Ti processed by warm ECAP and cold rolling [J]. Materials Science Engineering A, 2003, 343(1−2): 43−50.

[6] SHIN D H, KIM I, KIM J. Deformation mechanism of pure Ti during equal channel angular pressing [J]. Metals and Materials International, 2002, 8(6): 513−518.

[7] ZHAO X, FU W, YANG S, et al. Microstructure and properties of pure titanium processed by equal-channel angular pressing at room temperature [J]. Scripta Materialia, 2008, 59(5): 542−545.

[8] WANG Y, CHEN M, ZHOU F, et al. High tensile ductility in a nanostructured metal [J]. Nature, 2002, 419: 912−915.

[9] LEE Y B, SHIN D H, PARK K T, et al. Effect of annealing temperature on microstructures and mechanical properties of a 5083 Al alloy deformed at cryogenic temperature [J]. Scripta Materialia, 2004, 51(4): 355−359.

[10] VENKATESAN M, VENKATACHALAM P, RAVISANKAR R, et al. Effect of cold and cryo rolling on microstructure and mechanical properties of 6012 Al alloy [C]// International Conference on Advanced Materials and Composites (ICAMC). 2007: 496−504.

[11] HUANG Y, PRANGNELL P B. The effect of cryogenic temperature and change in deformation mode on the limiting grain size in a severely deformed dilute aluminium alloy [J]. Acta Materialia, 2008, 56(7): 1619−1632.

[12] AGNEW S R, HORTON J A, LILLO T M, et al. Enhanced ductility in strongly textured magnesium produced by equal channel angular processing [J]. Scripta Materialia, 2004, 50(3): 377−381.

[13] AGNEW S R, MEHROTRA P, LILLO T M, et al. Crystallographic texture evolution of three wrought magnesium alloys during equal channel angular extrusion [J]. Materials Science Engineering A, 2005, 408(1−2): 72−78.

[14] ZENG Z, JONSSON S, ROVEN H J. The effects of deformation conditions on microstructure and texture of commercially pure Ti [J]. Acta Materialia, 2009, 57(19): 5822−5833.

[15] NEMAT-NASSER S, GUO W G, CHENG J Y. Mechanical properties and deformation mechanisms of a commercially pure titanium [J]. Acta Materialia, 1999, 47(13): 3705−3720.

[16] KOCKS U K, TOME C N. WENK H R. Texture and anisotropy [M]. Cambridge: Cambridge Univ Press, 1998.

[17] WAGNER F, BOZZOLO N, Van LANDUYT O, et al. Evolution of recrystallisation texture and microstructure in low alloyed titanium sheets [J]. Acta Materialia, 2002, 50(5): 1245−1259.

[18] SUWAS S, BEAUSIR B, TOTH L S, et al. Texture evolution in commercially pure titanium after warm equal channel angular extrusion [J]. Acta Materialia, 2011, 59(3): 1121−1133.

[19] JUNG Y I, LEE M H, PARK J Y, et al. Simple approach to the mechanical anisotropy of cold-rolled zirconium alloys [J]. Metals and Materials International, 2009, 15(5): 803−807.

[20] LIM H K, KIM D H, LEE J Y, et al. Effects of rolling condition on the tensile properties of Mg-MM-Sn-Al-Zn alloy [J]. Metals and Materials International, 2009, 15(2): 337−343.

[21] AHN S H, CHUN Y B, YU S H, et al. Microstructural refinement and deformation mode of Ti under cryogenic channel die compression [J]. Materials Science Engineering A, 2010, 528(1): 165−171.

[22] CHUN Y B, YU S H, SEMIATIN S L, et al. Effect of deformation twinning on microstructure and texture evolution during cold rolling of CP-titanium [J]. Materials Science Engineering A, 2005, 398(1−2): 209−219.

[23] PAUL H, DRIVER J H, WAJDA W. Strain hardening and microstructure evolution of channel-die compressed aluminium bicrystals [J] Materials Science Engineering A, 2008, 477(1−2): 282−294.

[24] NAVE M D, BARNETT M R. Microstructures and textures of pure magnesium deformed in plane-strain compression [J]. Scripta Materialia, 2004, 51(9): 881−885.

[25] RAPPERPORT E J, HARTLEY C S. Deformation modes of zirconium at 77, 575, and 1 075 K [J]. Metallurgical Society of AIME, 1960, 218: 869−877.

[26] CHUN Y B, BATTAINI M, DAVIES C H J, et al. Distribution characteristics of in-grain misorientation axes in cold-rolled commercially pure titanium and their correlation with active slip modes [J]. Metallurgical and Materials Transactions A, 2010, 41A(13): 3473−3487.

[27] ALEXANDROV I V. Developing SPD methods for processing bulk nanostructured materials with enhanced properties [J]. Metals and Materials International, 2001, 7(5): 565−57.

[28] LIANG W, YANG D, HUANG X, et al. Micro-mechanisms of plastic deformation of two-phase TiAl-base alloy at room temperature [J]. Progress in Natural Science, 1998, 8(4): 485−487

[29] AKHTAR A. Basal slip in zirconium [J]. Acta Metallurgica, 1973, 21(1): 1−11.

[30] FIELD R D, HARTWIG K T, NECKER C T, et al. Equal-channel angular extrusion of beryllium [J]. Metallurgical and Materials Transactions A, 2002, 33(3): 965−972.

[31] LIU Q, HUANG S, LLOYD D J, et al. Microstructure and strength of commercial purity aluminium (AA 1200) cold-rolled to large strains [J]. Acta Materialia, 2002, 50(15): 3789−3802.

[32] LI Y S, TAO N R, LU K. Microstructural evolution and nanostructure formation in copper during dynamic plastic deformation at cryogenic temperatures [J]. Acta Materialia, 2008, 56(5−6): 230−241.